PCCP

Accepted Manuscript

ROYAL SOCIETY OF CHEMISTRY

www.rsc.org/pccp

Journal Name

ARTICLE TYPE

Strange kinetics of bulk-mediated diffusion on lipid bilayers

Diego Krapf,[*a,b] Grace Campagnola,[c] Kanti Nepal,[b] and Olve B. Peersen[c]

Diffusion at solid-liquid interfaces is crucial in many technological and biophysical processes. Although its behavior seems deceivingly simple, recent studies showing passive superdiffusive transport suggest diffusion on surfaces may hide rich complexities. In particular, bulk-mediated diffusion occurs when molecules are transiently released from the surface to perform three-dimensional excursions into the liquid bulk. This phenomenon bears the dichotomy where a molecule always return to the surface but the mean jump length is infinite. Such behavior is associated with a breakdown of the central limit theorem and weak ergodicity breaking. Here, we use single-particle tracking to study the statistics of bulk-mediated diffusion on a supported lipid bilayer. We find that the time-averaged mean square displacement (MSD) of individual trajectories, the archetypal measure in diffusion processes, does not converge to the ensemble MSD but it remains a random variable, even in the long observation-time limit. The distribution of time averages is shown to agree with a Lévy flight model. Our results also unravel intriguing anomalies in the statistics of displacements. The time averaged MSD is shown to depend on experimental time and investigations of fractional moments show a scaling $\langle |r(t)|^q \rangle \sim t^{q\nu(q)}$ with non-linear exponents, i.e. $\nu(q) \neq \text{const}$. This type of behavior is termed strong anomalous diffusion and is rare among experimental observations.

1 Introduction

Processes at solid-liquid interfaces play important roles across multiple fields. In particular surface diffusion and diffusion-controlled reactions have key functions in life sciences and biomedical technologies[1]. For example, surface reactions are of utmost importance in the development of implant biomaterials[2,3], affinity chromatography methods[4], and biosensors as well as in blood-contacting devices[5] such as heart valves and hemodialysis membranes. In cell biology biomolecular recognition and reactions on surfaces are essential for a vast array of physiological functions. The importance of molecular films in biology has been discussed for more than a century[6]. In fact, most biochemical reactions in cells take place at interfaces instead of in solution. Diffusion-controlled reactions often involve a search for a reactive target with the goal of minimizing the search time[7–9].

The random motion of a particle is usually characterized by the mean squared displacement (MSD). In its simplest form, diffusion processes can be described by Brownian motion, which in two dimensions (2D) manifests a linear MSD $\langle r^2(t) \rangle = 4Dt$, where D is the diffusion coefficient. However, diffusion at solid-liquid interfaces can exhibit rich complexities[10–14]. Systems with a non-linear MSD $\langle r^2(t) \rangle = K_\alpha t^\alpha$ display anomalous diffusion, where a slower-than-linear growth, i.e $\alpha < 1$, indicates subdiffusion; and faster-than-linear growth, $\alpha > 1$, indicates superdiffusion. Most importantly, anomalous diffusion alters reaction kinetics because the diffusion properties control the rate of molecular encounters[15,16].

A widespread feature of molecules diffusing at the solid-liquid interface involves the desorption of molecules from the surface into the liquid phase. Molecules will diffuse in three dimensions (3D) until they reach the interface again and readsorb. This intermittent process where molecules alternate between 2D and 3D phases is known as bulk-mediated diffusion and has been previously analyzed in terms of scaling arguments[17], simulations[18,19], and analytical approaches[20]. The first experimental study that probed bulk-mediated diffusion involved the dynamics of adsorbate molecules in porous glass studied by field-cycling NMR relaxometry[21]. Recently bulk-mediated diffusion was experimentally observed in systems of vastly different nature including organic molecules at chemically coated interfaces[12,22], polymer-surface interactions[23], and membrane-targeting domains on both supported lipid bilayers[24,25] and the plasma membrane of living

a Department of Electrical and Computer Engineering, Colorado State University, Fort Collins, CO 80523, USA; E-mail: krapf@engr.colostate.edu
b School of Biomedical Engineering, Colorado State University, Fort Collins, CO 80523, USA.
c Department of Biochemistry and Molecular Biology, Colorado State University, Fort Collins, CO 80523, USA.

cells[26]. Diffusion as measured on the surface is strongly influenced by the statistics of excursion times. On each excursion a random distance is covered on the surface, which scales in probability as the square root of the return time ($\langle r^2(t) \rangle = 4D_b t$). The first return time to the surface has interesting properties[27]. The most fundamental of these properties is the dichotomy between mean first return time and probability of return. On one hand, the mean first return time is infinite due to its heavy tail distribution $p(t) \sim t^{-1.5}$. On the other hand, a particle always returns to the surface, that is the probability of return is one. In terms of probability theory one would say the particle returns to the surface almost surely. To place the problem in real context, if we consider a generic protein that alternates between a lipid bilayer and a water-based solution, the probability that it returns to the surface within less than 50 ms after it reached a 10-nm height is 99.75%[25]. Another interesting scenario is provided by a cylindrical surface. In this case the MSD features a plateau, balancing increasingly long jumps with a decreasing return probability.[28].

A diffusion process where long jumps with a heavy-tail distribution occur is known as Lévy walk[29]. In such a random walk, jumps are performed at a velocity that might depend on the jump distance[30,31]. If the long jumps take place instantaneously, the process is known as Lévy flight[32]. Lévy walks have traditionally received more attention than flights because instantaneous jumps are not realistic. However, in the limit where bulk diffusion is orders of magnitude faster than surface diffusion, $D_b >> D_s$, a Lévy walk can be approximated as a Lévy flight, at least within short time scales. This regime is found to be the most relevant for experimental observations of bulk-mediated diffusion.

Both Lévy flights and walks are superdiffusive when the probability density of jump distances scales as $p(r) \sim r^{-(1+\beta)}$ with $\beta \leq 2$. We recently reported that the motion of membrane-targeting domains on lipid bilayers is superdiffusive due to bulk excursions[25]. In these experiments, the MSD grows faster-than-linear when it is measured over an ensemble of molecules, that is the average is performed by employing a single displacement for each trajectory at any given time. Nevertheless, when the average is performed over time, i.e. by averaging all the displacements observed along a trajectory, the MSD is linear in lag time. This observation contradicts the ergodic hypothesis, one of the cornerstones of statistical mechanics, which states that ensemble averages and long-time averages of individual trajectories are equivalent. A similar behavior is found in subdiffusive continuous time random walks (CTRWs), where the ensemble-averaged MSD follows a power law t^α, but the time-averaged MSD is linear[33,34]. In the CTRW, the non-ergodic property is rooted in the system not being stationary. Alike, molecular crowding conditions were predicted to introduce long-tailed distributions in both the unbinding times from the surface to the bulk and the rebinding times, which cause weak ergodicity breaking[35]. Such strange kinetics where the random walk exhibits different scaling properties depending on whether it is averaged over time or over an ensemble poses intriguing questions regarding its statistics. Beyond the MSD, the distribution of displacements also deviates from "normal" diffusion. The central limit theorem (CLT) warrants that the displacements of Brownian motion have a Gaussian distribution. However, in some types of

anomalous diffusion models, the CLT breaks down and the distribution of displacements is no longer Gaussian. For example, in a CTRW or when a particle diffuses in a fractal structure, the increments are not independent and thus the CLT does not hold. In a Lévy flight the CLT breaks down because the increments can have infinite variance[17,20].

Here we investigate the kinetics of membrane-targeting C2 domains on lipid bilayers using single-particle tracking. This system exhibits superdiffusive behavior in the ensemble-averaged MSD but normal scaling in the time-averaged MSD. Weak ergodicity breaking predicts large fluctuations in the time-averaged MSD of individual trajectories. Thus we examine the fluctuations in the MSD and find that it remains a random variable even in the long time limit. In contrast to the CTRW model, the increments of bulk-mediated diffusion are shown to be stationary, but the statistics of the motion still depend on experimental time. It is found that when the MSD is averaged over both time and ensemble, it does not converge to a finite value, but it increases with experimental time. Thus, if the diffusion coefficient were estimated using the MSD slope, it would increase as the experimental time increases. The experimental results for bulk-mediated diffusion are found to agree with a Lévy flight model using both analytical approaches and numerical simulations. Interestingly we also find the system exhibits strong anomalous diffusion[36], i.e., the fractional moments are not characterized by a linear scaling exponent as in most diffusion processes.

2 Materials and methods

2.1 Preparation of supported lipid bilayers

Lipid bilayers were prepared as described elsewhere[25]. In brief, chloroform-suspended 18:1 (Δ9-Cis) PC (DOPC) and 18:1 PS (DOPS) were mixed at a ratio of 3:1. The phospholipid mixture was vacuum dried overnight and resuspended in imaging buffer (50 mM HEPES, 75 mM NaCl, 1 mM MgCl$_2$, 2 mM tris(2-carboxyethyl)phosphine (TCEP), 200 μM CaCl$_2$) to a final concentration of 3 mM followed by probe sonication to form sonicated unilamellar vesicles (SUVs)[37]. A solution of SUVs (1.5-mM lipid) in 0.5 M NaCl and imaging buffer was introduced into a perfusion chamber (CoverWell, Grace Bio-Labs model PC8R-1.0) and incubated for one hour at 4°C. The surface was then rinsed with imaging buffer multiple times prior to addition of protein sample.

2.2 Protein expression, purification, and labeling

An expression plasmid containing the ybbr-Synaptotagmin 7 (Syt7) C2A gene[38] was transformed into *Escherichia coli* BL21-CodonPlus(DE3) competent cells. Cells were grown at 37°C to an OD$_{600}$ of 0.6 and then induced to express protein with 0.5 mM IPTG for 6 hours at room temperature. The harvested cells were lysed at 18,000 lb/in^2 in a microfluidizer in a buffer containing 50 mM Tris, pH 7.5, 400 mM NaCl and centrifuged at 17,000 rpm. The clarified lysate was loaded onto a 5-ml GSTrap FF column (GE Healthcare LifeSciences, Pittsburgh, PA) followed by gradient elution with 50 mM Tris, pH 8.0, 100 mM NaCl, and 10 mM glutathione. Fractions containing protein were pooled and di-

luted to reduce the salt to less than 0.1 M prior to loading onto a HiTrap Q HP column (GE Healthcare LifeSciences, Pittsburgh, PA) and eluting with a linear gradient to 1 M NaCl in 25 mM Tris, pH 8.5, 20%(vol/vol) glycerol, and 0.02%(wt/vol) NaN$_3$. A portion of the purified protein was subjected to thrombin cleavage to remove the GST tag and then separated using a Superdex 200 gel filtration column (GE Healthcare LifeSciences, Pittsburgh, PA) equilibrated in 50 mM Tris, pH 7.5 and 100 mM NaCl.

20 mM CoASH (New England Biolabs, Ipswich, MA) in 400 mM Tris, pH 7.5 was mixed with 20 mM Atto-565 maleimide (ATTO-TEC, Siegen, Germany) in dimethylformamide and incubated at 30°C overnight to form Atto-565 CoA, then diluted 10 fold with 5 mM DTT, 10 mM Tris pH 7.5 to quench the reaction. ybbr-Syt7 C2A was labeled with the Atto-565 via SFP synthase (4*/*-phosphopantetheinyl transferase). Samples were dialyzed against 1 L of 50 mM HEPES, pH 7.0, 75 mM NaCl, 4 mM MgCl$_2$ and 5% glycerol overnight at 4°C, and then concentrated to 10 μM.

2.3 Imaging and single-particle tracking

Proteins were added to the imaging buffer to a final concentration of 75 pM. Then, the perfusion chamber was filled with the solution. The perfusion chambers were 9 mm in diameter and 0.9-mm deep, holding a volume of ≈ 60 μl. Imaging was performed at room temperature without replacing the solution, so that there was always protein present in the bulk solution and the surface concentration could reach a steady state.

All images were acquired using an objective-type total internal reflection fluorescence microscope (TIRFM) as described previously[10,39]. A 561 nm laser line was used as excitation source. A back-illuminated electron-multiplied charge coupled device (EM-CCD) camera (Andor iXon DU-888) liquid-cooled to -85°C, with an electronic gain of 300 was used. In order to maintain constant focus during the whole imaging time we employed an autofocus system (CRISP, Applied Scientific Instrumentation, Eugene, OR) in combination with a piezoelectric stage (Z-100, Mad City Labs, Madison, WI). Videos were acquired at a frame rate of 20 frames/s using Andor IQ 2.3 software and saved as 16-bit tiff files. The images were filtered using a Gaussian kernel with a standard deviation of 1.0 pixel in ImageJ. Single-particle tracking of Atto-C2 was performed in MATLAB using the u-track algorithm developed by Jaqaman et al.[40].

3 Experimental Results

3.1 Fluctuations in time-averaged MSD

We tracked the motion of membrane-targeting C2A domains[25], fluorescently labeled with Atto-565, on a supported lipid bilayer. Imaging was done in a home-built total internal reflection (TIRF) microscope under continuous illumination at 20 frames/s. Single-particle tracking is performed under conditions where the surface density is low enough to enable connections of long jumps while avoiding misconnections due to crossover between trajectories. Figure 1 shows an example of single-molecule trajectories during 10 seconds. As a first step, we characterize the diffusion by analyzing the MSD as a function of lag time. For each individual
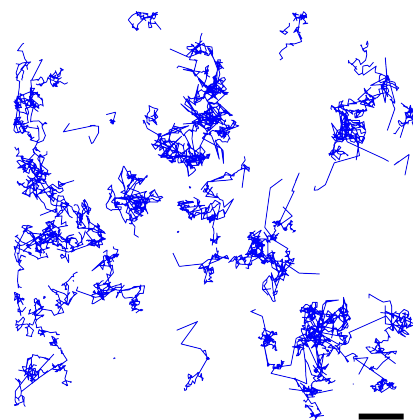

Fig. 1 Single particle tracking of membrane-targeting C2 domains. Individual trajectories are collected during 10 seconds in a 50×50 μm^2 window. Scale bar 5 μm.

trajectory, the time-averaged MSD (TA-MSD) is calculated as

$$\overline{\delta^2(\Delta)} = \frac{1}{t-\Delta}\int_0^{t-\Delta}[\mathbf{r}(\tau+\Delta) - \mathbf{r}(\tau)]^2 d\tau, \qquad (1)$$

where Δ is the lag time, t the experimental time, and $\mathbf{r}$ the two-dimensional position of a particle. Across the manuscript we employ brackets to denote the ensemble average of an observable $\langle \cdot \rangle$ and an overline to denote time averages $\overline{\cdot}$. Figure 2(a) shows that, within experimental error, the TA-MSD of individual trajectories is linear in lag-time, resembling pure Brownian motion. In two dimensions, the MSD of a Brownian particle is determined by the diffusion coefficient D via the relation $\overline{\delta^2(\Delta)} = 4D\Delta$, but Fig. 2(a) shows that the TA-MSD exhibits broad fluctuations. In ergodic systems, the time-averaged MSD converges to the ensemble average. In other words the time-averaged MSD can be used to consistently estimate the diffusion coefficient of a molecule. However, the large scattering seen Fig. 2(a) indicates the time-averaged diffusion coefficient of individual molecules is a random variable, with no apparent convergence. This observation suggests weak ergodicity is broken in the sense that time and ensemble averages do not converge to the same values[34].
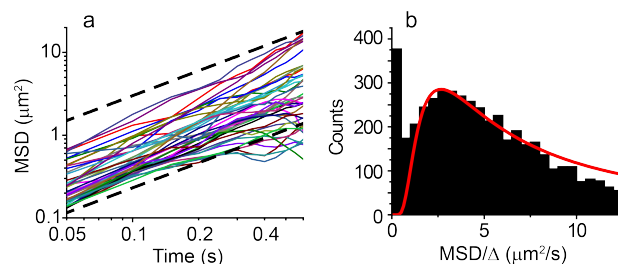

Fig. 2 Scattering of the estimated diffusion coefficients of individual trajectories. (a) The time-averaged MSD of individual trajectories, $\overline{\delta^2(\Delta)}$, displays large fluctuations indicating that the MSD does not self average. 40 randomly selected trajectories are presented in a log-log plot. The dashed lines are guides to the eye with $\overline{\delta^2(\Delta)} \sim \Delta$. The experimental time of all trajectories is 1.3 s. (b) Distribution of the MSD slopes for C2 domains. The apparent diffusion coefficient can be calculated from the MSD slope, $MSD/\Delta = 4D$. The thick red line shows the prediction by a bulk-mediated diffusion model as explained in the text.
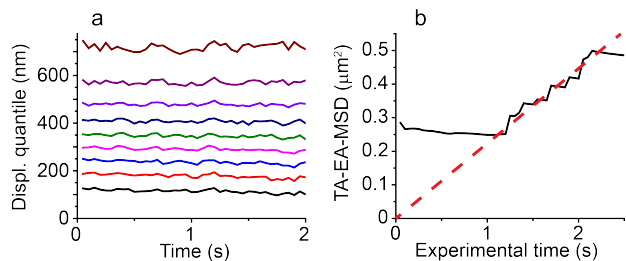
Fig. 3 Temporal properties of the MSD of membrane-targeting C2 domains. (a) 10-quantile lines of 50-ms increments of the C2 domain trajectories. Nine lines are shown for the fractions $k = 0.1$, 0.2, ..., 0.9, indicating the values that divide the increments into 10 equally-populated subsets, each subset comprising a 10th of the data points. The quantile lines are parallel, indicating the increments are stationary. (b) Time-averaged ensemble-averaged MSD (TA-EA-MSD) as a function of observation time for a 50-ms lag time. In order to compute the TA-EA MSD, all the displacements of all trajectories up to time t are averaged. Discrete jumps are observed, which increase the MSD with experimental time.

Given that the TA-MSD is linear in lag time, one is tempted to find the diffusion coefficient of individual molecules from linear regression of the MSD trace. Figure 2(b) shows the distribution of the slope of the TA-MSD, i.e. $\overline{\delta^2}/\Delta$, obtained from 5,187 trajectories. The distribution shows two different populations. A peak with very low diffusivities is apparent (sample mean $\langle \overline{\delta^2}/\Delta \rangle = 0.006 \ \mu\text{m}^2/\text{s}$). This population has a narrow distribution and it is attributed to particles that are immobilized and do not exhibit any motion. A second population with high diffusivities has the characteristic large variations noted in Fig. 2(a), with a mode at $2.7 \pm 0.1 \ \mu\text{m}^2/\text{s}$ but a sample mean $\langle \overline{\delta^2}/\Delta \rangle = 7.3 \ \mu\text{m}^2/\text{s}$. When particles perform long jumps, a trajectory can be truncated and traces with higher diffusivities are lost. It is thus expected that the true distribution of MSDs is even broader because experimental tracking is biased towards lower diffusivities.

3.2 Stationarity and dependence on experimental time

It is important to establish whether the diffusion process evolves with time. Further, ergodicity is defined only for stationarity processes and thus we test whether the non-ergodic motion is rooted in the increments not being stationary. One way to check stationarity of the increments is to compute the quantiles as a function of time. If the quantile lines are parallel then we can infer that the process is stationary [41]. Figure 3(a) shows the 10-quantile lines of the increments for lag times of 50 ms. The quantile lines appear to be parallel, suggesting the distribution of increments does not change over time. Therefore we can conclude that the process is stationary.

Even though the increments are stationary, the statistics of the diffusion process depends on experimental time. This effect is observed in the average of the time-averaged MSD, i.e., the time- and ensemble-averaged MSD (TA-EA-MSD, $\langle \overline{\delta^2} \rangle$). The TA-EA-MSD is simply the cumulative moving average of the square displacements, over different trajectories and for all times up to the experimental time. Figure 3(b) shows the TA-EA-MSD for $\Delta = 50$ ms as a function of experimental time measured for 3,130 tra-

jectories. The MSD does not appear to converge to any given value; instead it exhibits random jumps, so that it experiences an overall increase with experimental time. In ergodic systems, the TA-EA-MSD exhibits fluctuations around the mean, which become smaller as the available experimental time becomes longer due to better statistics. That type of noise is different from the behavior observed here because ergodicity would warrant the TA-EA-MSD converges to a finite value. The observed MSD increase is not monotonic and it decreases smoothly between jumps. Nevertheless, the rate of decrease of the MSD is much smaller than the average rate of increase due to the discrete jumps and thus, in probability, the MSD increases with time. As a consequence, if the ensemble-averaged MSD were employed to estimate a diffusion coefficient, then the coefficient would not be constant, but it would increase with experimental time.

3.3 Strong anomalous diffusion

So far, we have characterized the dynamics of molecules using the MSD and observed that the TA-MSD $\overline{\delta^2}$ does not converge to the ensemble-averaged MSD $\langle r^2(t) \rangle$. However, one may desire to characterize the motion beyond the second moment. In particular, the fractional moments $\langle |r(t)|^q \rangle$ with $q > 0$ provide useful insight. For Brownian motion as well as many anomalous diffusion processes $\langle |r(t)|^q \rangle \sim t^{q\nu}$. As long as ν is a constant, all moments are described by a scaling exponent linear in the order q and the process is scale invariant such that the propagator at different times is $P(x,t) = t^{-\nu} f(x/t^\nu)$ [36]. For example, in Brownian motion $\nu = 1/2$ and $f(\cdot)$ is a Gaussian function.

The process is said to exhibit strong anomalous diffusion when ν is not constant [13,36],

$$\langle |r(t)|^q \rangle \sim t^{q\nu(q)}. \tag{2}$$

Strong anomalous diffusion has been shown theoretically and via numerical simulations in a variety of systems including the motion of tracer particles in a running sandpile model [42], the occupation times of renewal processes [43], and flow fields [36] among others [44–46]. In these processes, a piecewise linear scaling is found for $q\nu(q)$. Experimental observation of strong anomalous diffusion has remained rather elusive. To the best of our knowledge, so far it has only been observed in the superdiffusive transport of polymer particles inside living cancer cells [47]. Figure 4(a-d) shows ensemble-averaged moments of the two-dimensional displacements of C2 domains, which are computed by averaging over all available trajectories $\langle |\mathbf{r}(t) - \mathbf{r}(0)|^q \rangle$. Two regimes are visible in all the moments. At short times, the fractional moments exhibit the behavior expected for Brownian motion, $\langle |r(t)|^q \rangle \sim t^{q/2}$, but at long times the moments "misbehave". Two solid lines are shown in each panel of Fig. 4(a-d): a shallow line with $\langle |r(t)|^q \rangle \sim t^{q/2}$ and a steeper line with $\langle |r(t)|^q \rangle \sim t^q$. For short times the agreement with a Brownian motion model ($q\nu(q) = q/2$) is evident. However, this is not the case for the long-time regime. In this regime, as the order q increases, the logarithmic slopes of the moments also increase. Figure 5 shows $\nu(q)$ as a function of q for both the short and long times. We see that the scaling exponent at short times does not show significant deviations
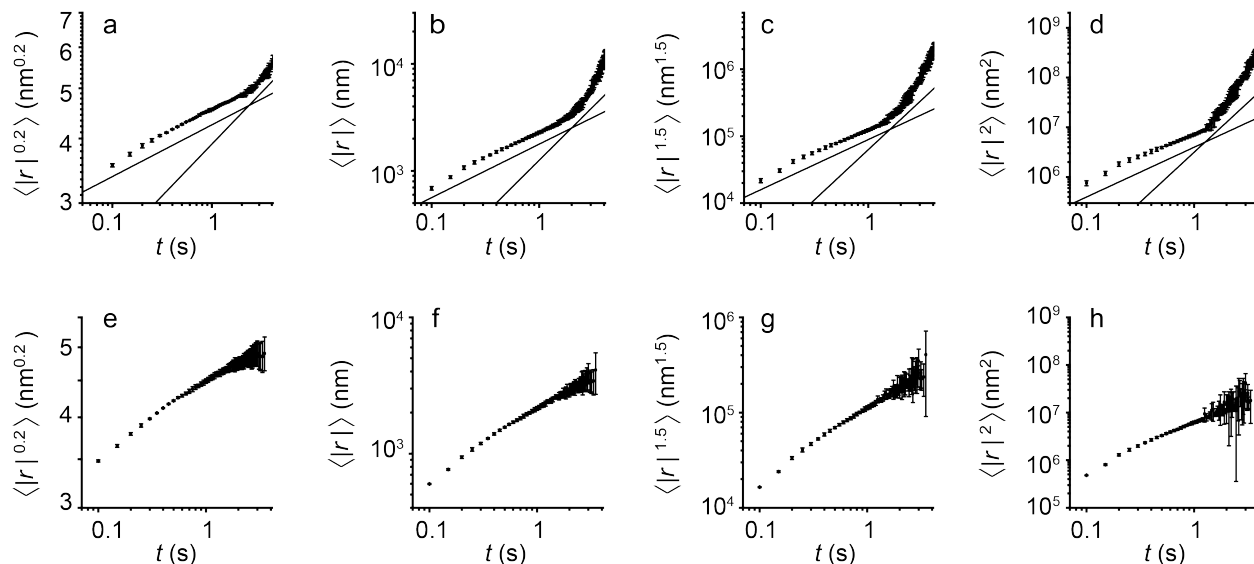
Fig. 4 Ensemble-averaged q^{th} moment of membrane-targeting C2 domains. (a-d) Moments are computed for $q = 0.2, 1, 1.5, 2$. The solid lines provide guides to the eye to $\langle |r(t)|^q \rangle \sim t^{q/2}$ and $\langle |r(t)|^q \rangle \sim t^q$, i.e. $\nu = 1/2$ (Brownian motion) and $\nu = 1$ (superdiffusion). (e-h) The same fractional moments are computed when the 3% longest displacements are excluded from the data analysis.
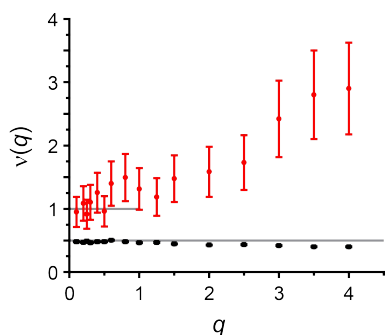

Fig. 5 The scaling exponent $q\nu(q)$ exhibits piecewise behavior at long times. At short times (lower black squares) $\nu(q) \approx 0.5$, but at long times (upper red circles) the behavior is very different and $\nu(q)$ is not constant. Instead $\nu(q)$ increases with the order q when $q > 1$. The gray lines indicate the expected $\nu(q)$ behavior of the fractional order exponent for Brownian motion and the Lévy flight model in the regime $0 < q < 1$.

from $q\nu(q) = q/2$ but in the long-time regime $\nu(q)$ is not constant. In this time regime, $q\nu(q) = q$ for the lower order moments and $\nu(q) > 1$ for the higher orders, which indicates strong anomalous diffusion. In our measurements, strong anomalous diffusion is caused by rare long jumps, i.e., by bulk excursions. When the large displacements are excluded from the analysis, the fractional moments display normal behavior. Figure 4(e-h) shows the fractional moments when only the displacements below a 97% cutoff are considered. We observe that in this case $\langle |r(t)|^q \rangle \sim t^{q/2}$, that is, the fractional moments without the long jumps scale with time as expected from Brownian motion.

4 Theoretical model

4.1 Fluctuations in the time averages

We have previously shown[25] that membrane-targeting domains can transiently dissociate from the lipid bilayer to perform bulk

excursions. During these excursions, a molecule undergoes three-dimensional diffusion until it readsorbs on the surface. Within the bulk phase, the height z is modeled as a one-dimensional random walk and thus the first return time distribution satisfies $p(t_b) \sim t_b^{-1.5}$, where the first return time t_b represents the time the particle spends in the bulk during a single jump. A sketch of the model is shown in Fig. 6. A simple derivation[27] leads to a one-sided Lévy distribution of index $1/2$, also known as a Lévy-Smirnov distribution,

$$p(t_b) = z_0 \left(4\pi D_b t_b^3 \right)^{-1/2} \exp\left(-z_0^2 / 4 D_b t_b \right), \tag{3}$$

where D_b is the diffusion coefficient in the bulk, and z_0 is a scaling constant with units of length. Then, the distances on the surface covered during bulk excursions are two-dimensional Cauchy random variables[17,20,25]

$$p(\mathbf{r}) = \frac{\gamma}{2\pi \left(r^2 + \gamma^2 \right)^{3/2}}, \tag{4}$$

where γ is a constant with units of length. Interestingly, the expected values of both the first return time and the displacement diverge. Therefore, we expect that the time-averaged MSD is governed by extreme values. Namely, because the TA-MSD is determined by individual long jumps, it remains a random variable, even though observation times may be long.

Let us first derive the distribution of time averages from intuitive scaling arguments. Given that one individual long jump determines the TA-MSD of an individual trajectory, each TA-MSD scales as the longest displacement within the trajectory,

$$\overline{\delta^2} \sim \frac{1}{t} \max\left\{ r_i^2 \right\}, \tag{5}$$

where r_i are the individual measured displacements. From Eq. (4), we can calculate the probability density of squared dis-
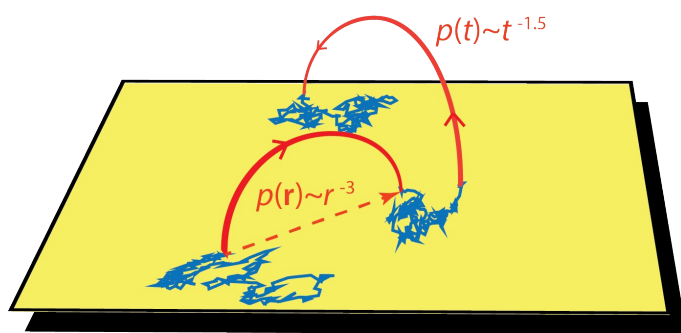
Fig. 6 Sketch of the bulk-mediated diffusion model. A molecule alternates between periods of 2D and 3D diffusion. The excursions into the bulk are considered as surface jumps with a heavy-tail distribution $p(\mathbf{r}) \sim r^{-3}$. In theory, the sojourn time in the bulk phase are asymptotically power-law distributed, $p(t) \sim t^{-1.5}$, but in practice jumps are observed to take place faster than the frame rate.

placements and that of TA-MSD. Defining $s = r^2$, we obtain the distribution $p(s) = 0.5\gamma(s + \gamma^2)^{-3/2}$. Then, we find the distribution of $\overline{\delta^2}$ from the cumulative distribution function of the squared displacements $F_S(s)$. Namely, $F_{MSD}\left(\overline{\delta^2}\right) = \left[F_S(t\overline{\delta^2})\right]^t$ because the displacements are independent and identically distributed. Thus

$$p\left(\overline{\delta^2}\right) \sim t^2 \left(1 - \frac{\gamma}{\sqrt{t\overline{\delta^2} + \gamma^2}}\right)^{t-1} \frac{0.5\gamma}{\left(t\overline{\delta^2} + \gamma^2\right)^{3/2}}, \qquad (6)$$

where for the sake of simplicity we take time t as the number of time intervals, i.e. the number of measured displacements. In the limit of large MSDs we have $t\overline{\delta^2} \gg \gamma^2$ and Eq. (6) simplifies to

$$p\left(\overline{\delta^2}\right) \sim 0.5 t^{1/2} \gamma \left(\overline{\delta^2}\right)^{-3/2}. \qquad (7)$$

These simple scaling arguments yield a distribution of TA-MSD that has a power law tail with an exponent 3/2.

Now, we follow the derivation by Froemberg and Barkai to find the whole distribution of TA-MSDs[48]. In order to simplify the analysis we focus on a one-dimensional Lévy flight but the extension to two dimensions is straightforward. Again the displacements are Cauchy distributed (Eq. 4), albeit in one dimension,

$$p(x_i) = \frac{\gamma}{\pi \left(x_i^2 + \gamma^2\right)}, \qquad (8)$$

and the square displacements $y = x^2$ are distributed according to

$$p(y) = \frac{\gamma}{\pi \left(y + \gamma^2\right)\sqrt{y}} \sim y^{-3/2}. \qquad (9)$$

where $y \geq 0$. The displacements after time Δ are $x_\Delta = \sum_i^\Delta x_i$, with a characteristic function $\phi(k) = \exp(-\gamma\Delta|x|)$. Thus $p(x_\Delta) = \gamma t [\pi(x_\Delta^2 + \gamma^2 t^2)]^{-1}$, also a Cauchy distribution with a scale parameter $\gamma\Delta$. This behavior is due to the fact that the Cauchy distribution is stable, namely a symmetric Lévy stable distribution of index 1. Therefore, we can solve for $\Delta = 1$ and our results are still valid for any lag time after rescaling $\gamma \to \gamma\Delta$.

As in Eq. 1, the TA-MSD at a lag time Δ, measured over a time

t, is[48]

$$\overline{\delta^2(\Delta)} = \frac{1}{t-\Delta} \sum_{i=1}^{t-\Delta} (x_{i+\Delta} - x_i)^2$$

$$\overset{d}{\approx} \frac{\Delta}{t} \sum_{i=1}^{t} x_i^2, \qquad (10)$$

where the approximation holds for $t \gg 1$. We next define the variable $\zeta = t\overline{\delta^2}/\Delta \overset{d}{\approx} \sum_{i=1}^{t} x_i^2$, which is a sum of independent and identically distributed (i.i.d.) random variables y_i. Given that the variance of y_i diverges, the central limit theorem breaks down and the distribution of ζ is found using the generalized central limit theorem[49]. The Laplace transform of the distribution of $y = x^2$ (see Eq. 9) is

$$p(u_y) = \exp\left(\gamma^2 u_y\right) \text{erfc}\left(\gamma\sqrt{u_y}\right)$$

$$\approx 1 - \frac{2\gamma}{\sqrt{\pi}}\sqrt{u_y} + O(u_y)$$

$$\approx \exp\left(-\frac{2\gamma}{\sqrt{\pi}}\sqrt{u_y}\right), \qquad (11)$$

where $\text{erfc}(\cdot)$ is the complementary error function. We are concerned with large values of y and therefore we only keep the first term in the series expansion in Eq. (11), that is we only consider the small u_y limit in Laplace domain. The distribution of ζ in the large t limit is found in Laplace domain

$$p(u_\zeta) = \exp\left(-\frac{2\gamma t}{\sqrt{\pi}}\sqrt{u_\zeta}\right). \qquad (12)$$

The inverse Laplace transform yields

$$p(\zeta) = \frac{\pi}{2(\gamma t)^2} L_{1/2,1}\left[\frac{\pi}{2(\gamma t)^2}\zeta\right]$$

$$= \left(\frac{1}{2\pi c^2 \zeta^3}\right)^{1/2} \exp\left(-\frac{1}{2c^2\zeta}\right), \qquad (13)$$

where $L_{1/2,1}(\xi)$ is again the Lévy-Smirnov distribution and we introduced the constant $c = \sqrt{(\pi/2)}/\gamma t$. We can then change variables to obtain the distribution of the slope of the TA-MSD. By defining $\xi = \zeta/t = \overline{\delta^2}/\Delta$, Eq. 13 simplifies to

$$p(\xi) = \left(\frac{\gamma^2 t}{\pi^2 \xi^3}\right)^{1/2} \exp\left(-\frac{\gamma^2 t}{\pi\xi}\right). \qquad (14)$$

Thus we find that the probability density function of the TA-MSD is a Lévy-Smirnov distribution with scale parameter $2\gamma^2 t/\pi$. Recall that we derived this distribution for t and Δ in number of frames. In agreement with the scaling arguments discussed above, $p(\xi) \sim \xi^{-3/2}$. Importantly, the moments of this distribution diverge, causing large variations in the TA-MSD measurements as observed in Fig. 2(a).

4.2 Fractional moments

Our Lévy flight model involves a tail in the distribution of displacements that scales as $p(\mathbf{r}) \sim r^{-3}$ at long distances. Therefore, the qth moment diverges for $q \geq 1$. Explicitly,

$$\langle |r(t)|^q \rangle \sim \begin{cases} t^q, & q < 1 \\ \infty, & q \geq 1. \end{cases} \tag{15}$$

Of course this result is not realistic. The problem arises in the approximation that bulk excursions take place instantaneously. While the approximation is good within our experimental times, it does not hold for very long jumps, thus placing a bound on the higher order moments. In fact, for bulk-mediated surface diffusion the Cauchy distribution (Eq. 4) has a natural Gaussian cutoff that emerges at longer times than those probed in our study[20]. Precise mathematical analysis that includes the time incurred by a bulk mediated jump would lead to the correct higher order moments[13,50]. However, a simple model leading to Eq. (15) yield some useful insights. In particular, we can see that there is a critical order $q_c = 1$ below which $\nu(q) = 1$. Furthermore, for values $q < q_c$, the fractional moments yield superdiffusive behavior, i.e $\nu(q) > 1/2$ as would be determined by Brownian motion. Above this critical value, the fractional moments increase above 1. The piecewise behavior is the fingerprint of strong anomalous diffusion as observed in Fig. 5.

5 Numerical Simulations

We test the predictions of our model using numerical simulations and compare them to the experimental data. Our simulations intend to model a process where molecules diffuse on a two dimensional surface and undergo dissociation into the bulk phase. Dissociation is considered as a Poisson process and the particle goes through 3D diffusion in the bulk until it finds its way back to the surface. 5000 realizations were simulated off-lattice where tracers perform a random walk with Gaussian displacements in two dimensions, and at random times the tracer performs bulk excursions[25]. The sojourn times within the surface are exponentially distributed with a mean of 10 and the surface diffusion coefficient is taken to be $D_s = 0.5$. The return times from bulk excursions are drawn from a distribution $\psi(t_b) = (4\pi t_b^3)^{-1/2}\exp(-1/4t_b)$ (see Eq. 3). Then the jump distances are Gaussian with variance $\sigma_b^2 = 2t_b$.

Similar to the experiments on lipid bilayers, the TA-MSD of the simulations exhibit a broad scattering. Figure 7(a) shows the distribution of TA-MSDs for the individual realizations. Overlaid on this distribution in Fig. 7(a), equation 14 shows good agreement with the MSD distribution.

In our derivation of the distribution of the TA-MSDs, we have employed the Cauchy distribution (Eq. 4) for the displacements. This equation ignores the Gaussian component in the distribution of displacements that arises due to the diffusive motion on the surface[25]. As seen in Fig. 7(a), this approximation does not alter the distribution, at least in the long measurement time limit. The reason is that, as discussed above, the MSD is governed by the large displacements, i.e., the tail of the distributions. Further, we would achieve the same results (Eq. 14) if we only consider the
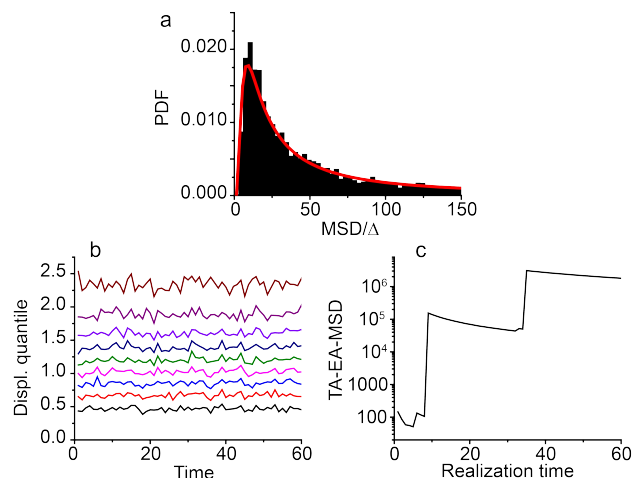

Fig. 7 Model where a tracer diffuses on a plane and is allowed to dissociate to performed bulk excursions until readsorbing to the surface. (a) Probability density function of the distribution of TA-MSD slopes obtained from 5,000 realizations, where each realization includes 500 displacements. The predicted Levy distribution for the MSD is also shown as a solid red line. (b) 10-quantiles of the increments of the realizations. The quantile lines are parallel, indicating that the process is stationary as expected[41]. (c) The ensemble average of the TA-MSD exhibits jump discontinuities increasing the MSD when the realization time increases.

power law tail of the propagator, $p(\mathbf{r}) \sim |r|^{-3}$ and find the Laplace transform using the Tauberian theorem[49,51].

6 Discussion

In a similar fashion to the numerical simulations of bulk-mediated diffusion, Eq. 14 is used to model the experimental results for membrane-targeting C2 domains (red solid line in Fig. 2(b)). Even though the agreement between our bulk-mediated diffusion model and the experimental results is satisfactory, the tail in the MSD distribution of C2 domains decreases faster than predicted by the model. This effect is caused by an artificial truncation of the distribution of displacements caused by the tracking algorithm[25]. Namely, if a particle experiences a very long jump, it is not possible to make frame-to-frame connections with reasonable confidence and thus trajectories are cropped missing the long displacements and in turn the large diffusivities.

The increments in the motion of C2 domains on a lipid bilayer are shown to be stationary but the MSD depends on the experimental time (Fig. 3). This behavior is also observed in our numerical simulations. The increments in the simulations are stationary (Fig. 7(b)) as the displacements are simulated with the same time-independent stochastic process. However, the TA-EA-MSD of the numerical simulations also shows a strong dependence on realization time (Fig. 7(c)). In agreement with the C2 data, the simulations MSD show discrete jumps in the time series. Also here, the MSD average increases in probability with realization time.

The discontinuities in the MSD as a function of experimental time can be conceptually understood in terms of the same mechanism that causes weak ergodicity breaking. As discussed before, the estimated diffusivities of individual trajectories are governed

by extreme displacements. Recall that the reason for the lack of self-averaging is the existence of one displacement in the trajectory that is likely much larger than all others and thus the MSD depends on this individual displacement. In the same way, at a given time t, a jump may occur among all the molecules such that it is much larger than all the displacements observed thus far. When such an event takes place the TA-EA-MSD increases sharply due to the contribution of one long jump. After a very large jump occurs, the relative weight of that individual long jump diminishes because more data points become available. Thus, following a jump discontinuity the MSD decreases with experimental time. The MSD continues to decrease until the next jump discontinuity takes place.

We observed that, in probability, the sample mean of the TA-MSD increases with experimental time. This is also observed in the theoretical distribution of the TA-MSD (Eq. 14), which involves a scale parameter that explicitly depends on the experimental time. Even though the expected value of the TA-MSD diverges we can estimate how the MSD increases with experimental time by evaluating other measures of central tendency, such as the theoretical mode and median. Both of these measures scale linearly with time, namely.

$$\text{mode}_\xi = \frac{2\gamma^2}{3\pi} t \qquad (16)$$

and

$$\text{median}_\xi = \frac{\gamma^2}{\pi \left[\text{erfc}^{-1}(1/2)\right]} t \qquad (17)$$

where $\text{erfc}^{-1}(\cdot)$ is the inverse complementary error function. Thus we expect the average of the TA-MSD to increase in probability linearly with experimental time as observed in Fig. 3(b).

In this manuscript we employed the fractional moments and showed that the system exhibits strong anomalous diffusion. The fractional moments are only rarely used in the diffusion literature. Nevertheless, these moments can be very useful in the analysis of bulk mediated diffusion. When the trajectories are modeled as Lévy flights the theoretical MSD diverges and its use in the analysis of motion challenging. This is not the case for fractional moments with $q < 1$, where the theoretical moment is finite and no discontinuities are observed. Thus low order moments become a useful tool to study phenomena such as superdiffusion.

Our data shows that the common practice of finding diffusivities from time averaged MSD in membranes should be approached with care. We find that weak ergodicity is broken and as a consequence the MSD of individual trajectories are random variables even in the long time limit. In other words, the MSD from individual trajectories are not reproducible. Furthermore, the ensemble mean of the time-averages is not a reliable measure because it depends on experimental time. Careful analysis indicates that as the available measurement time becomes longer, the apparent diffusion coefficient increases. In order to deal with this subtlety we propose that, when bulk excursions are evident in the data, parameters are extracted from the distributions instead of using either time or ensemble averages. We have previously shown that it is feasible to obtain both the surface diffusion co-efficient and the scale parameter γ from the distribution of displacements when the data sample is large enough[25].

7 Conclusions

We have shown that bulk-mediated diffusion can be accurately modeled as a Lévy flight. The Lévy flight concept yields superdiffusive dynamics with complex strange kinetics, in particular because the time averaged MSD does not converge to the ensemble average. Thus the process exhibits weak ergodicity breaking. The time-averaged MSD of individual trajectories is governed by individual long jumps and, as a consequence, it remains a random variable. We have shown that the MSD also depends on experimental time and thus it does not provide a consistent estimator of the diffusion coefficient. The long time asymptotic of the displacement fractional moments has the signature of superdiffusive behavior both for low and high orders. Moreover, the Lévy flight model predicts strong anomalous diffusion, a phenomenon that deals with non-linear scaling exponents of the fractional displacement moments. We have experimentally observed this anomalous behavior in the motion of membrane-targeting domains on supported lipid bilayers using single-particle tracking. Future work will explore the effects of temperature and macromolecular crowding on bulk-mediated dynamics. Given the broad applicability of bulk mediated diffusion, we foresee these anomalies can be observed in many complex systems.

Acknowledgements

References

1. D. G. Castner and B. D. Ratner, *Surf. Sci.*, 2002, **500**, 28–60.
2. B. D. Ratner, A. S. Hoffman, F. J. Schoen and J. E. Lemons, *Biomaterials science: an introduction to materials in medicine*, Academic press, 2004.
3. L. L. Hench and J. M. Polak, *Science*, 2002, **295**, 1014–1017.
4. G. S. Chaga, *J. Biochem. Biophys. Methods*, 2001, **49**, 313–334.
5. J. Courtney, N. Lamba, S. Sundaram and C. Forbes, *Biomaterials*, 1994, **15**, 737–744.
6. J. Loeb, *Proteins and the theory of colloidal behavior*, McGraw-Hill, 1922.
7. P. Hänggi, P. Talkner and M. Borkovec, *Rev. Mod. Phys.*, 1990, **62**, 251.
8. M. A. Lomholt, T. Ambjörnsson and R. Metzler, *Phys. Rev. Lett.*, 2005, **95**, 260603.
9. O. Bénichou, C. Loverdo, M. Moreau and R. Voituriez, *Rev. Mod. Phys.*, 2011, **83**, 81.
10. A. V. Weigel, B. Simon, M. M. Tamkun and D. Krapf, *Proc. Natl. Acad. Sci. U.S.A.*, 2011, **108**, 6438–6443.

11 E. Barkai, Y. Garini and R. Metzler, *Phys. Today*, 2012, **65**, 29–35.

12 M. J. Skaug, J. Mabry and D. K. Schwartz, *Phys. Rev. Lett.*, 2013, **110**, 256101.

13 R. Metzler, J.-H. Jeon, A. G. Cherstvy and E. Barkai, *Phys. Chem. Chem. Phys.*, 2014, **16**, 24128–24164.

14 D. Krapf, *Curr. Top. Membr.*, 2015, **75**, 167–207.

15 M. F. Shlesinger, G. M. Zaslavsky and J. Klafter, *Nature*, 1993, **363**, 31–37.

16 O. Bénichou, C. Chevalier, J. Klafter, B. Meyer and R. Voituriez, *Nat. Chem.*, 2010, **2**, 472–477.

17 O. V. Bychuk and B. O'Shaughnessy, *Phys. Rev. Lett.*, 1995, **74**, 1795.

18 O. V. Bychuk and B. O'Shaughnessy, *J. Chem. Phys.*, 1994, **101**, 772–780.

19 J. A. Revelli, C. E. Budde, D. Prato and H. S. Wio, *New J. Phys.*, 2005, **7**, 16.

20 A. V. Chechkin, I. M. Zaid, M. A. Lomholt, I. M. Sokolov and R. Metzler, *Phys. Rev. E*, 2012, **86**, 041101.

21 S. Stapf, R. Kimmich and R.-O. Seitter, *Phys. Rev. Lett.*, 1995, **75**, 2855.

22 M. J. Skaug, A. M. Lacasta, L. Ramirez-Piscina, J. M. Sancho, K. Lindenberg and D. K. Schwartz, *Soft Matter*, 2014, **10**, 753–759.

23 C. Yu, J. Guan, K. Chen, S. C. Bae and S. Granick, *ACS Nano*, 2013, **7**, 9735–9742.

24 J. D. Knight and J. J. Falke, *Biophys. J.*, 2009, **96**, 566–582.

25 G. Campagnola, K. Nepal, B. W. Schroder, O. B. Peersen and D. Krapf, *Sci. Rep.*, 2015, **5**, 17721–17721.

26 M. Yasui, S. Matsuoka and M. Ueda, *PLoS Comput. Biol.*, 2014, **10**, e1003817–e1003817.

27 S. Redner, *A guide to first-passage processes*, Cambridge University Press, 2001.

28 A. V. Chechkin, I. M. Zaid, M. A. Lomholt, I. M. Sokolov and R. Metzler, *Phys. Rev. E*, 2009, **79**, 040105.

29 M. F. Shlesinger and J. Klafter, *On growth and form*, Springer, 1986, pp. 279–283.

30 M. Shlesinger, B. West and J. Klafter, *Phys. Rev. Lett.*, 1987, **58**, 1100.

31 J. Klafter, M. F. Shlesinger and G. Zumofen, *Phys. Today*, 1996, **49**, 33–39.

32 B. B. Mandelbrot, *The fractal geometry of nature*, W. H. Freeman, 1982.

33 A. Lubelski, I. M. Sokolov and J. Klafter, *Phys. Rev. Lett.*, 2008, **100**, 250602.

34 Y. He, S. Burov, R. Metzler and E. Barkai, *Phys. Rev. Lett.*, 2008, **101**, 058101.

35 M. A. Lomholt, I. M. Zaid and R. Metzler, *Phys. Rev. Lett.*, 2007, **98**, 200603.

36 P. Castiglione, A. Mazzino, P. Muratore-Ginanneschi and A. Vulpiani, *Physica D*, 1999, **134**, 75–93.

37 J. A. Corbin, R. A. Dirkx and J. J. Falke, *Biochemistry*, 2004, **43**, 16161–16173.

38 J. Yin, A. J. Lin, D. E. Golan and C. T. Walsh, *Nat. Protocols*, 2006, **1**, 280.

39 A. V. Weigel, M. M. Tamkun and D. Krapf, *Proc. Natl. Acad. Sci. U.S.A.*, 2013, **110**, E4591–E4600.

40 K. Jaqaman, D. Loerke, M. Mettlen, H. Kuwata, S. Grinstein, S. L. Schmid and G. Danuser, *Nat. Methods*, 2008, **5**, 695–702.

41 J. Janczura and A. Weron, *J. Chem. Phys.*, 2015, **142**, 144103.

42 B. Carreras, V. Lynch, D. Newman and G. Zaslavsky, *Phys. Rev. E*, 1999, **60**, 4770.

43 C. Godrèche and J. Luck, *J. Stat. Phys.*, 2001, **104**, 489–524.

44 K. Andersen, P. Castiglione, A. Mazzino and A. Vulpiani, *Eur. Phys. J. B*, 2000, **18**, 447–452.

45 E. Bacry, J. Delour and J.-F. Muzy, *Phys. Rev. E*, 2001, **64**, 026103.

46 R. Artuso and G. Cristadoro, *Phys. Rev. Lett.*, 2003, **90**, 244101.

47 N. Gal and D. Weihs, *Phys. Rev. E*, 2010, **81**, 020903.

48 D. Froemberg and E. Barkai, *Eur. Phys. J. B*, 2013, **86**, 1–13.

49 W. Feller, *An introduction to probability theory and its applications*, John Wiley & Sons, 2008, vol. 2.

50 A. Rebenshtok, S. Denisov, P. Hänggi and E. Barkai, *Phys. Rev. Lett.*, 2014, **112**, 110601.

51 J. Klafter and I. M. Sokolov, *First steps in random walks: from tools to applications*, OUP Oxford, 2011.